Investigation of a General Aviation
Differential Pressure Angle of Attack Probe[‡]

David F. Rogers
Professor of Aerospace Engineering (Emeritus)
Rogers Aerospace Engineering & Consulting
Annapolis, Maryland
dfr@nar-associates.com

Abstract

A wind tunnal calibration of a commerically available general aviation differential pressure angle of attack probe was conducted. Differential pressure varied linearly with pitch angle for each dynamic pressure tested. Beyond $\pm 6°$ of yaw angle, differential pressure rolled off rapidly with yaw angle. Normalizing differential pressure with dynamic pressure collapsed the differential pressure to a single curve for pitch. Similarly, normalizing differential pressure with the dynamic pressure collapsed the differential pressure to a single curve for yaw. Normalizing the differential pressure with dynamic pressure removes the effect of speed and density altitude when deriving angle of attack from differential pressure.

Normalizing the differential pressure using the pressure from the $45°$ probe surface similarly collapsed the differential pressure to single separate curves for both pitch and yaw. Differential pressure varied parabolically with pitch angle when normalized using the pressure from the $45°$ probe surface. For pitch angles above six degrees, a linear relation between differential pressure normalized with the pressure from the $45°$ probe surface and the square of the pitch angle provided an adequate approximation.

The typical two-point linear approximation based on two in-flight calibration points results in significant errors in displayed angle of attack. Moving the low angle of attack in-flight calibration point closer to the stall angle of attack reduces the displayed angle of attack error in the critical stall region. Using a four-point linear approximation significantly reduces the error in displayed angle of attack throughout the angle of attack range.

Combined pitch, yaw and roll results in sideslip, which produces significant error in displayed angle of attack based on calibration at zero yaw and roll.

[‡] This article is based on the AIAA Jounal of Aircraft paper, Rogers, David F., *Investigation of a General-Aviation Differential Pressure Angle-of-Attack Probe*, Journal of Aircraft, Vol. 50, No. 5 (2013), Sept-Oct. 2013, pp. 1668-1671 with further extensions.

Nomenclature

a	=	lift curve slope
b	=	wing span
C_L	=	aircraft lift coefficient
D	=	aircraft drag
e	=	Oswald efficiency factor
EAS	=	equivalent aircraft speed
f	=	aircraft equivalent parasite drag area
L	=	aircraft lift
$L/D_{\max}$	=	maximum lift to drag ratio
P_{fwd}	=	pressure on probe forward port
P_{45}	=	pressure on probe 45° surface
q	=	dynamic pressure
R^2	=	square of the correlation coefficient
S	=	wing reference area
V	=	true airspeed
V_{CC}	=	Carson cruise speed
$V_{L/D_{\max}}$	=	maximum lift to drag speed
$V_{P_{R_{\min}}}$	=	minimum power required speed
V_{stall}	=	stall speed
W	=	weight of the aircraft
α	=	angle of attack
α_{CC}	=	angle of attack for Carson cruise speed
$\alpha_{L/D_{\max}}$	=	angle of attack for $L/D_{\max}$
$\alpha_{P_{R_{\min}}}$	=	angle of attack for minimum power required
ϕ	=	roll angle
θ	=	wind tunnel pitch angle
ρ	=	density
ρ_{SL}	=	density at sea level
σ	=	ratio of the density at altitude to that at sea level, ρ/ρ_{SL}

Introduction

Recently there has been renewed interest in equipping light general aviation aircraft with angle of attack instrumentation. The Federal Aviation Administration has facilitated this effort by declaring the addition of angle of attack instrumentation as a minor modification provided that certain conditions are met. The key condition is: "The installation of the angle of attack system does not require interface with the existing pitot-static system; the installation does not require direct pressure input from the pitot-static system."[Sad11]. This requirement dictates that the angle of attack system stand alone.

The typical light general aviation angle of attack system measures a differential pressure and interprets the result as angle of attack. Because of flow field effects, in-flight calibration is necessary. Typically the differential pressure at two flight conditions, e.g., near stall and in cruise, are used as in-flight calibration points. The angle of attack is interpreted using a linear variation between the differential pressures at the two in-flight calibration points. A wind tunnel investigation was undertaken to determine the accuracy of this method.

The Probe

The probe tested is a typical commercial differential pressure angle of attack probe. Typically the probe is mounted on the bottom of the wing of a single engine aircraft, as shown in Figure 1, or on the underside of the nose of a twin engine aircraft. When mounted under the aircraft wing the probe extends forward and downward at a nominal 45° degree angle to the wing surface. Provision is provided to re-orientate the probe at 5° increments from 35° to 90° to aid in-flight calibration

Figure 1.   Angle of attack probe mounted under the wing.

The probe contains two pressure ports, each 0.1″ in diameter. One pressure port, called P_{fwd} in Figure 2, is nominally aligned with the airstream direction under the wing. In high speed cruise flight P_{fwd} nominally measures total pressure. The second pressure port, called P_{45} in Figure 2, is located on the flat 45° surface. The differential pressure $\Delta P = P_{fwd} - P_{45}$ is related to angle of attack. Conceptually, this is similar to the classical spherical or cylindrical based differential pressure angle of attack probe (see for example Gracey [Gra58] and Arend and Saunders [Are09] and the references therein).

The Wind Tunnel

The tests were conducted in the United States Naval Academy's open circuit induction or "Eiffel" wind tunnel. In this tunnel the discharge from the exit is returned to the inlet within the laboratory in which the tunnel is housed. The tunnel was designed to have low turbulence. Turbulence is controlled by using a contraction ratio of 9.6, a $1/4$ inch wide by six inch thick aluminum honeycomb screen at the entrance of the contraction section followed by four stainless steel 20×20 per inch mesh screens. Forty-five degree fillets are installed, beginning at the test section entrance and continuing through the test section into the diffuser to compensate for boundary layer growth. The ten foot long enclosed test section accommodates two balances. The upstream test section is equipped with a pyramidal balance while the downstream test section contains a sting balance. When the sting balance is in use the upstream model supports are removed and a flush plate fitted to the test section floor. The balance enclosure is sealed to equalize the enclosure pressure with the test section pressure. Hence, flow around the model supports is eliminated. The nominal test section size is $44w \times 31h$ inches. Dynamic pressure in the test section is measured using static pressure rings in the settling chamber just prior to the contraction and just upstream of the test section. The tunnel constant is 1.0303. The turbulence factor is 0.98.

The Tests

The angle of attack probe was mounted in the sting balance, as shown in Figure 3. The forward pressure port was aligned with the centerline of the test section at zero pitch and yaw angles. Pressure at the forward pressure port (P_{fwd}) and the pressure port on the 45° surface (P_{45}) were measured

Figure 2. Pressure port locations.

Figure 3. Angle of attack probe mounted in the wind tunnel.

4

on an alcohol manometer inclined at 29.6°. Pressure measurments were read with an accuracy of $0.05 \pm 0.025''$alcohol on the inclined scale. The tunnel dynamic pressure was read on a variable inclination inclined manometer. The accuracy of the variable inclination inclined manometer is $^1\!/_4$%. The manometer fluid was alcohol with a specific gravity of 0.811. The dynamic pressure was read to an accuracy of $0.05''$alc.

The parallel arm pitch mechanism on the sting balance maintained the P_{fwd} pressure port of the model in a three-dimensional space 2 inches in the flow direction $\times$ 4 inches wide and $\times$ $4^1\!/_2$ inches high in the center of the nominally 44×31 inch test section, for pitch and yaw angles of $\pm 24°$ and $\pm 20°$ respectively. Tunnel wall effects are considered negligible.

The tunnel was equipped with a computerized system to maintain constant dynamic pressure in the test section. Accuracy, varified by observation of the variable incidence alcohol dynamic pressure manometer, was within $\pm 0.1''$alc.

The Results

The probe was pitched through $\pm 6°$ at zero yaw and yawed through $\pm 6°$ at zero pitch at one degree intervals to establish a baseline. The pressure difference $P_{fwd} - P_{45}$ varied linearly with pitch angle and was constant with yaw angle throughout the limited test range.

Tests were conducted for a range of pitch and yaw angles at nominal dynamic pressures of 9.33, 15.35, 25.7 and 42.17 psf, which nominally correspond to equivalent airspeeds of 88.6, 113.6, 147.0, 188.3 fps. These dynamic pressures and equivalent airspeeds are within the range between stall and $V_{L/D\max}$ for typical light general aviation aircraft.
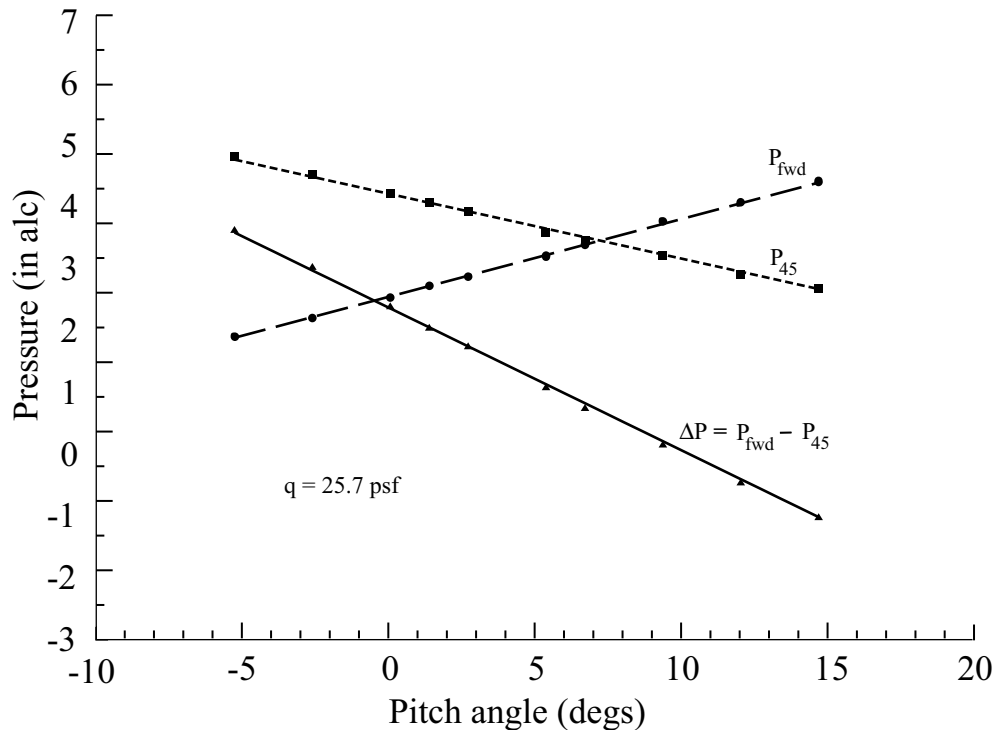

Figure 4.   Raw pitch data for P_{fwd}, P_{45} and $P_{fwd} - P_{45}$ for a nominal dynamic pressure of 25.7 lb psf.

Pitch

Figure 4 shows the raw data as read from the inclined manometer for P_{fwd}, P_{45} and $P_{fwd}-P_{45}$ as a function of pitch angle for a dynamic pressure of 25.7 psf. Clearly, these pressures vary linearly with pitch angle. The results for dynamic pressures of 9.33, 15.7 and 42.17 psf are similar. Figure 5 compares $P_{fwd}-P_{45}$ for dynamic pressures of 9.33, 15.7, 25.7 and 42.17 psf. As is easily seen, there is a significant effect of the dynamic pressure on the accuracy of the indicated angle of attack for a given differential pressure $P_{fwd}-P_{45}$. For example, if the differential pressure $P_{fwd}-P_{45}$ is $-1''$alc the corresponding angles of attack are 10.2, 11.2, 13.0 and 16 degrees for dynamic pressures of 9.33, 15.7, 25.7 and 42.17 psf. Significant error in the angle of attack results in the critical low speed/stall flight region.

As expected, and as shown in Figure 6, normalizing the differential pressure using the dynamic pressure collapses the data in Figure 5 to a single straight line. However, acquiring the dynamic pressure requires access to the aircraft pitot-static system, which is not acceptable to the Federal Aviation Administration (FAA) [Sad11] without significant certification effort and expense.

Yaw

Figure 7 shows the raw data as read from the inclined manometer for P_{fwd}, P_{45} and $P_{fwd}-P_{45}$ as a function of yaw angle for a dynamic pressure of 25.8 psf. Notice that the differential pressure is essentially constant for yaw angles of $\pm 6°$. The results for nominal dynamic pressures of 9.33, 15.7 and 42.17 psf are similar. Again, as with the pitch results, a significant dynamic pressure effect is observed.

Figure 8 shows that normalizing the results using the dynamic pressure collapses the data to a single curve although not as well as for pitch. Again, the normalized differential pressure is essentially constant for yaw angles of $\pm 6°$. However, it falls off significantly for yaw angles larger than $10°$. For example, from Figure 8 at a yaw of $+10°$ yields $(P_{fwd}-P_{45})/q = 0.27$. Using the normalized zero yaw and roll calibration curve for $(P_{fwd}-P_{45})/q = 0.27$ yields an angle of attack of $1°$, i.e., a $9°$ error in the displayed angle of attack. Furthermore, the displayed angle of attack is lower than the actual angle of attack which is non-conservative.
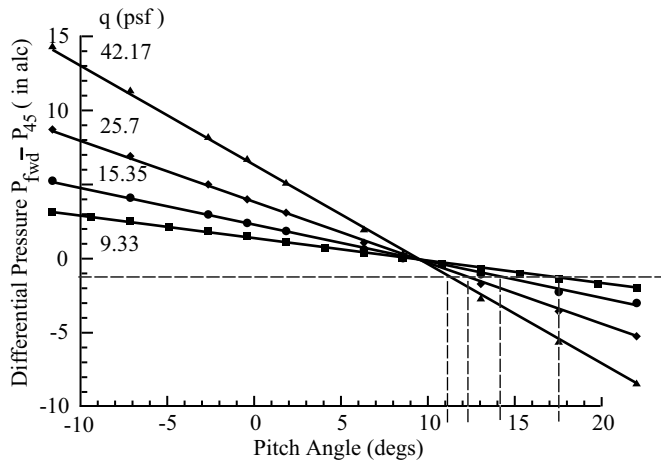

Figure 5. Comparison of the pitch differential pressure, $P_{fwd}-P_{45}$, for various dynamic pressures.
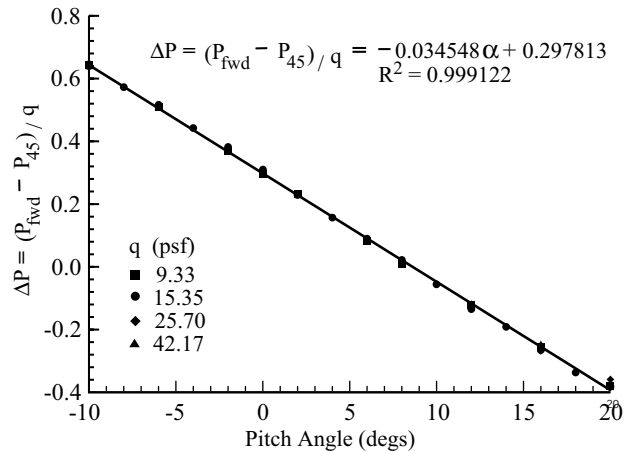

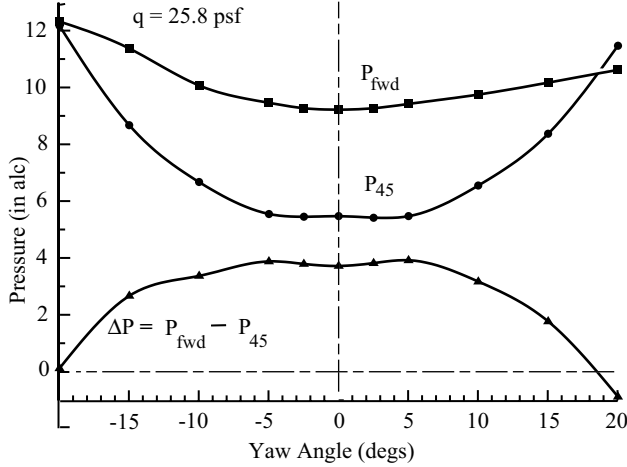**Figure 6.** Pitch differential pressure normalized by dynamic pressure $(P_{fwd}-P_{45})/q$.

Figure 7. Raw yaw data for P_{fwd}, P_{45} and $P_{fwd} - P_{45}$ for a nominal dynamic pressure of 25.8 psf.
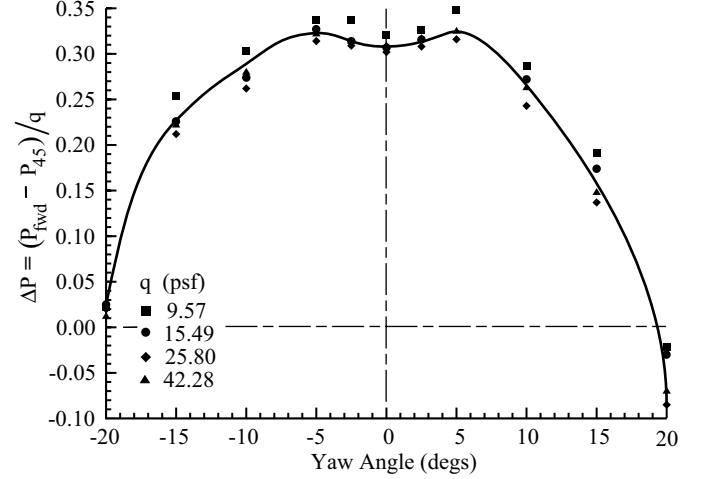

Figure 8. Yaw differential pressure normalized by dynamic pressure $(P_{fwd} - P_{45})/q$.

Flight Line

In order to determine the error in angle of attack it is necessary to determine the flight angle of attack as a function of flight conditions specifically as a function of equivalent airspeed (EAS). From

$$C_L = a\alpha = \frac{2W}{\rho_{\mathrm{SL}}(EAS)^2 S} \qquad \text{we have} \qquad \alpha = \frac{1}{a}\frac{2W}{\rho_{\mathrm{SL}}(EAS)^2 S} \tag{1}$$

In terms of the equivalent airspeed the dynamic pressure is given by

$$q = \tfrac{1}{2}\rho_{\mathrm{SL}}(EAS)^2 \tag{2}$$

Recall the equation for the normallized differential pressure for the angle of attack probe is

$$\frac{\Delta P}{q} = \frac{P_{\mathrm{fwd}} - P_{45}}{q} = m_1\alpha + b_1 = -0.034548\alpha + 0.297813 \tag{3}$$

From these three equations the differential pressure sensed by the angle of attack probe can be determined as a function of angle of attack as shown in Figure 9 and labelled "Flight Line". For typical angles of attack from high speed cruise to near stall the Flight Line varies approximately parabolically.

There are four angles of attack that are of importance to pilots of light general aviation aircraft ($W \leq 6000$ lbs). These are the stall angle of attack and those for maximum lift to drag ratio, minimum power required and economical high speed cruise, i.e., the Carson cruise speed [CAR82]. The stall angle of attack is important for an obvious reason: the pilot would like to avoid stalling the aircraft. The angle of attack for maximum lift to drag ratio is important because it represents both the condition for best glide and best range for a piston powered aircraft. The angle of attack for minimum power required represents the condition for maximum endurance as well as the dividing line between the regions of normal and reverse command. The Carson cruise angle of attack represents the optimal condition for high speed cruise with minimum increase in fuel flow per unit time. In each case, for a given aircraft configuration, these angles of attack depend only on aircraft design parameters and are independent of weight and altitude. To see this, consider the angle of attack for maximum lift to drag ratio. Recall that the true airspeed for $L/D_{\max}$ is

$$V_{L/D\max} = \left(\frac{2}{\sigma\rho_{\mathrm{SL}}}\frac{W}{b}\frac{1}{\sqrt{\pi f e}}\right)^{1/2} \tag{4}$$

7

or in terms of the square of the equivalent airspeed

$$(\text{EAS}_{L/D\text{max}})^2 = \frac{2}{\rho_{\text{SL}}} \frac{W}{b} \frac{1}{\sqrt{\pi f e}} \tag{5}$$

Rewriting Eq.(1) for L/D_{max} yields

$$(\text{EAS}_{L/D\text{max}})^2 = \frac{2}{a\alpha} \frac{1}{\rho_{\text{SL}}} \frac{W}{S} \tag{6}$$

Equating Eqs.(5 and 6) and solving for the angle of attack for L/D_{max} yields

$$\alpha_{L/D\text{max}} = \frac{1}{a} \frac{b}{S} \sqrt{\pi f e} \tag{7}$$

which, for a given aircraft configuration, depends only on aircraft design parameters and is independent of weight and altitude.

Similarly, recalling that the velocities for minimum power required and for Carson cruise [CAR82] are

$$V_{P_{R\text{min}}} = \frac{1}{\sqrt[4]{3}} V_{L/D\text{max}} \qquad \text{and} \qquad V_{\text{CC}} = \sqrt[4]{3} V_{L/D\text{max}}$$

the corresponding angles of attack are

$$\alpha_{P_{R\text{min}}} = \sqrt{3} V_{L/D\text{max}} \qquad \text{and} \qquad \alpha_{\text{CC}} = \frac{1}{\sqrt{3}} V_{L/D\text{max}} \tag{8}$$

For a typical light general aviation retractable gear aircraft with $a = 0.083/\text{deg}$, $b = 33.5$ ft, $S = 181$ ft^2, $f = 3.125$ ft^2 and $e = 0.56$ the angles of attack are

$$\alpha_{L/D\text{max}} = 5.23°; \qquad \alpha_{P_{R\text{min}}} = 9.06°; \qquad \alpha_{\text{CC}} = 3.02°$$

(see [ROG10] for additional information on the aircraft). These angles are shown on the flight line in Figure 9.

Effect of Two-Point Linear Calibration

Typically, simple differential pressure based angle of attack probes use a 2-point calibration with linear interpolation between the two calibration points, as previously mentioned. The dashed line in Figure 9 shows the resulting calibration line when the Carson speed and a speed 10% above stall speed are used as the calibration points. The gray shaded area illustrates the error in displayed angle
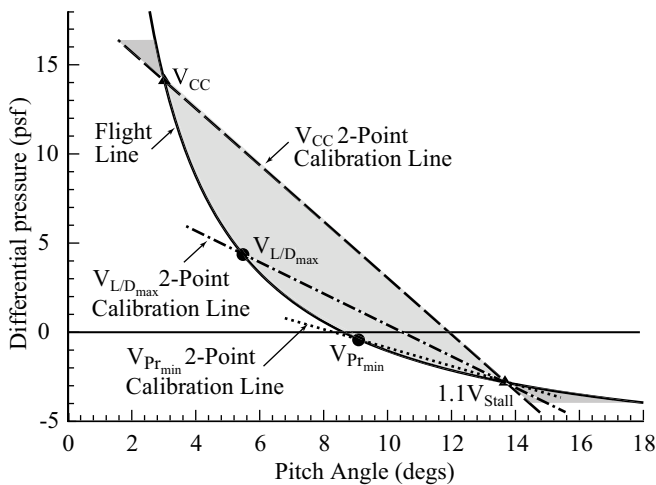

Figure 9. Flight line and the effect of 2-point linear calibration.
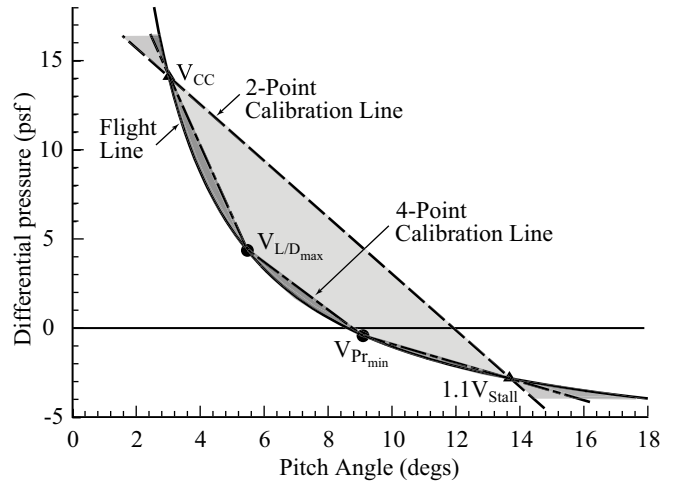

Figure 10. Comparison of 2-point and 4-point linear calibration.

of attack that results from this technique. This error can be significant. For example, at a differential pressure reading of 5 psf the actual angle of attack as read from the flight line is approximately 5.2° while the displayed angle of attack as determined by the calibration line is approximately 8.7°, an error of 3.5°. Between the calibration points the displayed angle of attack overestimates the actual angle of attack. At the calibration points the error reduces to zero. Outside of the calibration points, linear calibration underestimates the angle of attack. This is particular egregious in the stall region. As illustrated in Figure 9, moving the high speed calibration point closer to the stall region calibration point at $1.1V_{\text{stall}}$ reduces the error, as shown by the chain dashed line through $V_{L/D\text{max}}$ and the dotted line through $V_{P_{R_{\text{min}}}}$ and $1.1V_{\text{stall}}$, especially in the stall region. However, the error in the high speed region to the left of the flight line is increased.

An Improved Calibration Technique

Figure 9 suggests an improved calibration technique using four points with linear interpolation between the points. The result using V_{CC}, $V_{L/D\text{max}}$, $V_{P_{R_{\text{min}}}}$ and $1.1V_{\text{stall}}$ as the calibration points is shown in Figure 10, along with the 2-Point calibration. For comparison, the error between the flight line angle of attack and the 4-Point calibration is shown as a darker shaded area. As expected, the error in displayed angle of attack and the flight line angle of attack is considerably smaller.

Alternate Normalization Techniques

The calibration techniques mentioned above do not account for the dynamic pressure effects shown in Figure 5. Because the FAA does not consider an angle of attack system on a general aviation aircaft that accesses the aircraft pitot-static system (see [Sad11]) a minor alteration, an alternate method of normalizing the differential pressure independent of the aircraft pitot-static system is shown in Figure 11. Here, the differential pressure ($\Delta P = P_{\text{fwd}} - P_{45}$) is normalized using the pressure from the 45° surface. Figure 11 clearly shows that the results for all four dynamic pressures tested collapse into a single parabolic curve. Similar results, not shown, are obtained by normalizing P_{fwd} by P_{45}, i.e., P_{fwd}/P_{45}. Writing the equation for $\Delta P/P_{45}$ in Figure 11 as

$$\hat{a}\theta^2 + \hat{b}\theta + \hat{c} = 0 \tag{9}$$

where $\hat{a} = -0.001304$, $\hat{b} = -0.040428$, and $\hat{c} = 0.426844 - \Delta P/P_{45}$ the pitch angle, θ, which
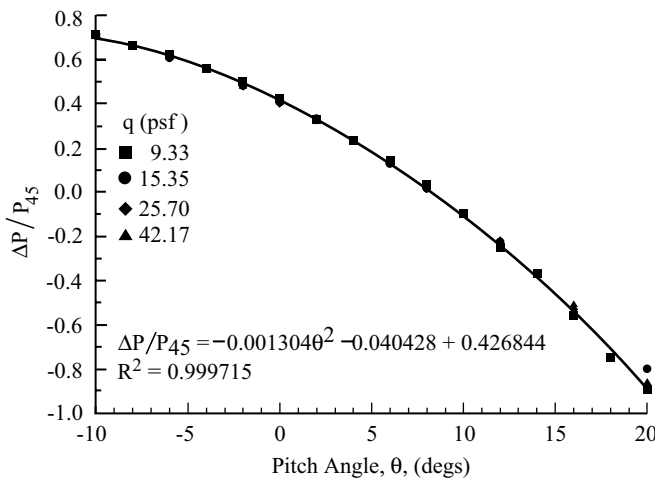

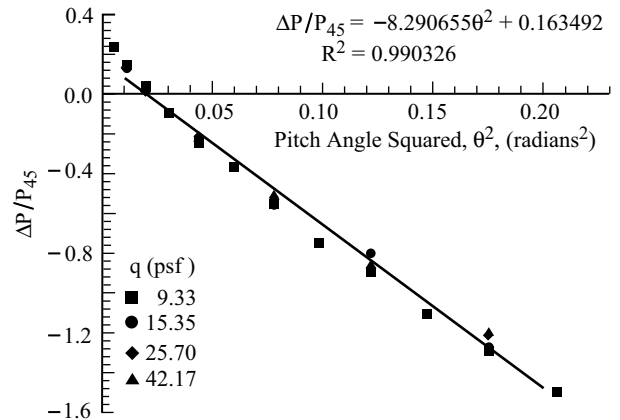**Figure 11.** Alternate method of normalizing the differential pressure.

Figure 12. Approximate variation of differential pressure with pitch angle squared.

corresponds to the aircraft angle of attack, α, is simply

$$\alpha = \theta = -15.5 \pm \sqrt{240.3 + 766.9\hat{c}} \tag{10}$$

Careful consideration must be given to insure that the resulting angle of attack is within the normal operating range for the particular aircraft. For example, for a non-aerobatic aircraft the angle of attack should be positive. It is suggested that in-flight calibration using the four points discussed above, specifically V_{CC}, $V_{L/D\max}$, $V_{P_{R\min}}$ and $1.1V_{\text{stall}}$, is adequate to provide an aircraft specific calibration.

The parabolic variation of $\Delta P/P_{45}$ with angle of attack suggests that assuming a linear variation of $\Delta P/P_{45}$ with the square of the angle of attack might be useful. Figure 12 shows the results for positive angles of attack greater than approximately six degrees. Figure 12 shows that the approximation is least accurate for low and medium angles of attack, i.e., for the cruise phase of flight, and reasonably accurate for higher angles of attack, i.e., in the critical flight regime approaching stall. Writing the equation in Figure 12 as

$$\bar{a}\theta^2 + \bar{c} = 0 \tag{11}$$

where $\bar{a} = -8.29065$ and $\bar{c} = 0.163492 - \Delta P/P_{45}$, the angle of attack and pitch angle are then simply

$$\alpha = \theta = \sqrt{\frac{(0.163492 - \dfrac{\Delta P}{P_{45}})}{0.8290655}} \tag{12}$$

The accuracy in the critical near stall regime is on the order of $\pm 0.5°$.

Combined Pitch, Yaw and Roll Effects

If the probe is not yawed or pitched but only rolled about the free stream direction, then there is little or no effect on the differential pressure measured and hence on the angle of attack indication. However, if the probe is simultaneously pitched and rolled then a yaw, or more properly a sideslip, results. Figure 13 illustrates this effect. In Figure 13 the probe has been pitched 25°, yawed 10° and rolled 45° for illustrative purposes. The flow direction is perpendicular to and into the image. Clearly, the effective yaw or sideslip is greater than 10°.

Simultaneous Pitch and Roll

Figure 14 shows that, when simutaneously pitched and rolled, for roll angles up to an order of 12–15° the error in normalized differential pressure is reasonably small. However, above these values the error increases significantly. For example, for a typical aircraft at the dynamic pressure of $25.91\,\text{psf}(\approx100\text{ MIAS})$ given in Figure 14 the angle of attack in level flight might be 8.5°. Recall that the angle of attack varies as $1/cos(\phi)$. If the aircaft is rolled (banked) to a 45° bank angle, then the angle of attack required to maintain level flight is $8.5/\cos(45) = 12°$. However, interpolating between the orange dots in Figure 14, the normalized differential pressure measured by the probe is approximately 0.1. The pitch (angle of attack), based on the zero yaw and roll calibration curve shown in black in Figure 14, interprets this pressure as approximately 6.6° (see Figure 11), a significant error. The system thus displays a much lower angle of attack. This is not conservation if the aircraft is close to stall.

Simultaneous Pitch and Yaw

Figure 15 illustrates, when simultaneously pitched and yawed, for yaw angles up to on the order of 7.5° that the error in the normalized differential pressure is again reasonably small. Above 7.5° the error increases dramatically, albeit in a conservative direction, i.e., the angle of attack display shows a value greater than the actual angle of attack. Again, using the typical aircraft cited above for an

Figure 13.   Angle of attack probe pitched 25°, yawed 10° and rolled 45°.
The viewpoint is directly into the image.

angle of attack in level flight of 8.5° and interpolating between the ×s in Figure 15 for a 15° yaw angle, the normalized differential pressure is approximately −0.21. The calibration curve for zero yaw and roll interprets this as an angle of attack of approximately 11.8°. This is still a significant error but conservative because it results in the display of an angle of attack larger than actual. For larger yaw angles, which are unlikely outside of aerobatic flight, the errors are considerably larger.

Comparing Figure 14 and Figure 15 shows that the effects of yaw and roll are opposite. Specifically, Figure 14 shows that as the probe is rolled while simultaneously pitched the normalized differential pressure increases with increasing roll angle. Hence, the displayed angle of attack is smaller than the angle of attack derived from the zero yaw and roll calibration curve represented by the solid black line. However, Figure 15 shows that as the probe is yawed while simultaneously pitched, the normalized differential pressure decreases with increasing yaw angle. Hence, the displayed angle of attack is larger than the angle of attack derived from the zero yaw and roll calibration line. This leads us to look at simulataneous pitch, yaw and roll.

Simultaneous Pitch, Yaw and Roll

Figure 16 shows the effects of simulataneously pitching, rolling and yawing the probe for roll angles of 15° and 30° and yaw angles of 5°, 10°, 15°, and 20° compared to the normalized differential pressure calibration curve for zero roll and yaw represented by the solid black line. As expected from Figures 14 and 15, the effect of moderate roll and yaw angles is mixed.

For a roll angle of 15° and yaw angles of 15° and 20° the displayed angle of attack derived from the zero yaw and roll calibration line is larger than the actual angle of attack. However, for yaw
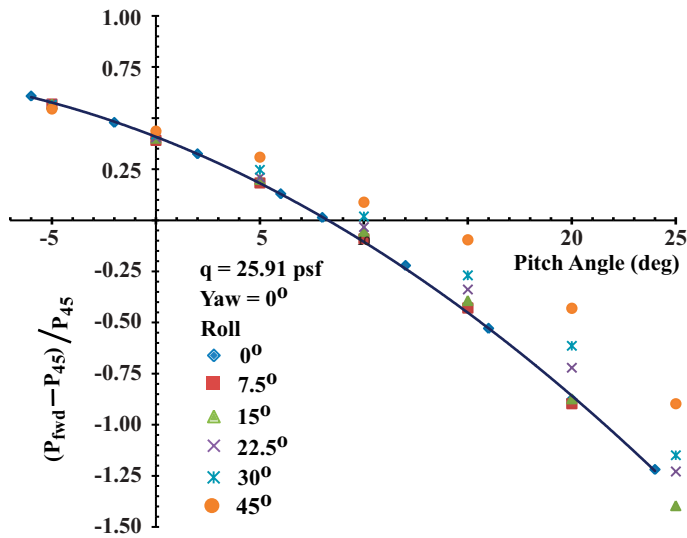
Figure 14. The effect of simultaneous pitch and roll on normalized differential pressure $(P_{fwd}-P_{45})/P_{45}$ for $q = 25.86$ psf.
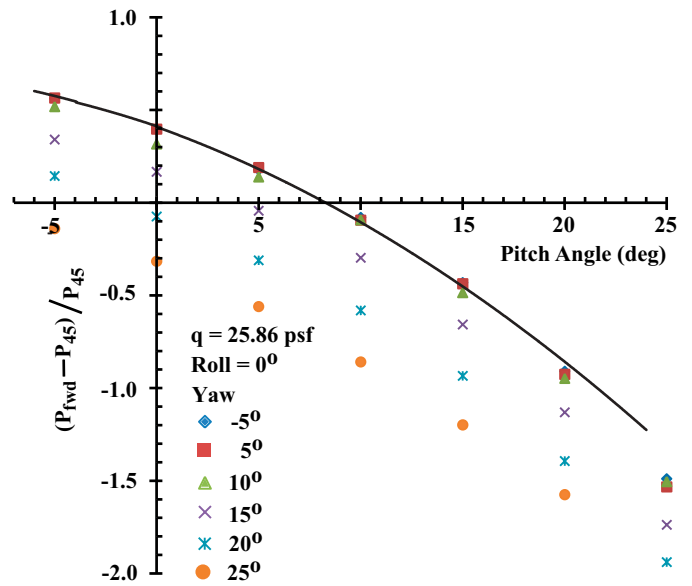

Figure 15. The effect of simultaneous pitch and yaw on normalized differential pressure $(P_{fwd}-P_{45})/P_{45}$ for $q = 25.86$ psf.

angles of 5° and 10° the displayed angle of attack is smaller than the actual angle of attack. Again, using a typical aircraft with a dynamic pressure of approximately 25.86 psf($\approx$ 100 MIAS) at zero yaw and pitch the angle of attack is 8.5°. Banked 30° the actual angle of attack is approximately 9.8°. From Figure 16b the displayed angle of attack is consistently smaller than the actual angle of attack.
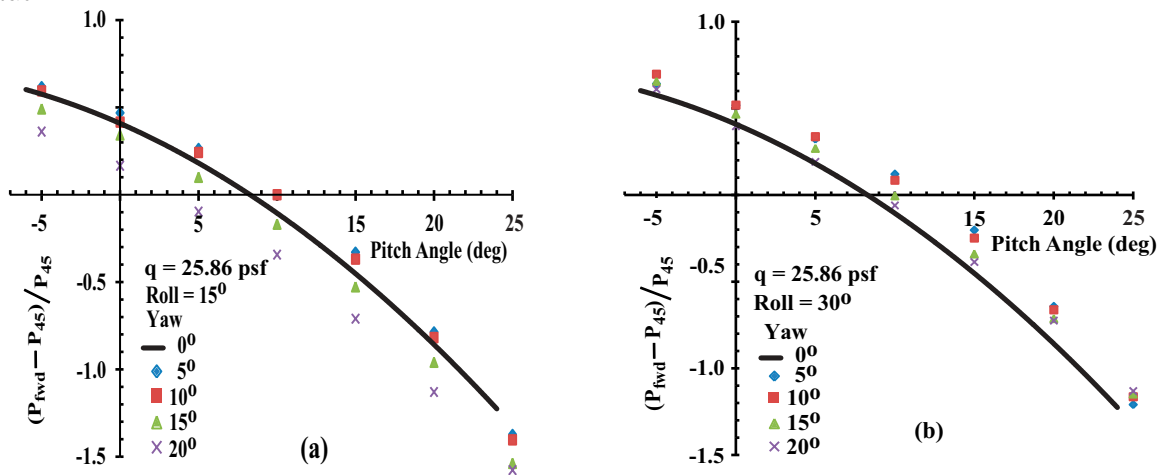

Figure 16. Effect of combine pitch, yaw and roll on the normalized differential pressure for a dynamic pressure of 25.86 psf≈100 MIAS; (a) roll = 15°, (b) = 30°

Conclusions

A wind tunnel calibration of a commerically available general aviation differential pressure angle of attack probe in both pitch and yaw was conducted. The differential pressure varied linearly with pitch angle for each dynamic pressure tested. The differential pressure was basically independent of yaw within $\pm 6°$. Beyond $\pm 6°$ the differential pressure rapidly rolled off, introducing significant errors beyond $\pm 10°$. The measured differential pressure was significantly affected by dynamic pressure. Normalizing the differential pressure by dynamic pressure collapsed the data to a single linear relation in pitch angle. It was discovered that normalizing the differential pressure by the pressure on the probe-inclined surface also collapsed the data but in this case to a single parabolic relation in terms of the pitch angle. Finally, it was discovered that in the range from approximately $V_{L/D\mathrm{max}}$ to stall a linear relation between $\Delta P/P_{45}$ with the square of the pitch angle provided an adequate approximation to the pitch angle.

The typical implementation of a differential pressure based angle of attack probe assumes a linear variation in angle of attack with differential pressure based on a 2-point in-flight calibration. Typically one calibration point is in cruise flight and the other near stall. This assumption results in significant errors in displayed angle of attack except at and near the calibration points. For angles of attack beyond the calibration points the displayed angle of attack is lower than the actual angle of attack. Between the calibration points the displayed angle of attack is higher than the actual angle of attack. Moving the high angle of attack calibration point closer to the stall angle of attack reduces the error in the stall region. Furthermore, moving the low angle of attack calibration point closer to the stall angle of attack also reduces the error in the critical stall region.

The wind tunnel tests suggest that a 4-point in-flight calibration procedure, using the speeds for Carson cruise [CAR82], maximum lift to drag ratio, power required minimum (maximum endurance) and 110% of stall, results in a significant reduction in displayed angle of attack throughout the angle of attack range.

Combined pitch, yaw and roll angle of attack yields mixed results when comparing displayed angle of attach and actual angle of attack for practical combined angles of yaw and bank.

References

Sad11　Letter from the FAA Small Airplane Directorate, Kansas City, KS, to DepotStar Inc. dated 15 December 2011.

Gra58　Gracey, W, "Summary of Methods of Measuring Angle of Attack on Aircraft," NACA TN-4351, August 1958.

Are09　Arend, D. J. and Saunders, J. D., "An Experimental Evaluation of the Performance of Two Combination Pitot Pressure Probes," NASA Technical Paper TP-2009-215632M, October 2009.

CAR82　Carson, B. H., "Fuel Efficiency of Small Aircraft," *Journal of Aircraft*, Vol. 19, 1982, pp. 473–479.

ROG10　Rogers, D. F.,"Flight Determination of Partial-Span-Flap Parasite Drag with Flap Deflection," *Journal of Aircraft*, Vol. 47, 2010, pp. 551–555.